

RESEARCH ARTICLE



CrossMark

3D tomatoes' localisation with monocular cameras using histogram filters

Sandro Costa Magalhães *,^{1,2}, Filipe Neves dos Santos ², António Paulo Moreira ^{1,2} and Jorge Dias ^{3,4}

¹Faculty of Engineering, University of Porto, Porto, Portugal.

²INESC TEC – Instituto de Engenharia de Sistemas e Computadores, Tecnologia e Ciência, Porto, Portugal.

³Institute of Systems and Robotics, Department of Electrical Engineering and Computers, University of Coimbra, Coimbra, Portugal.

⁴Khalifa University of Science, Technology, and Research, Abu Dhabi, United Emirates of Arabia (EUA).

*Corresponding author. E-mail: sandro.a.magalhaes@inesctec.pt.

Received: xx xxx xxx; **Revised:** xx xxx xxx; **Accepted:** xx xxx xxx

Keywords: 3D object detection, depth estimation, Bayes filter, robotic manipulator arms, statistical localisation

Abstract

Performing tasks in agriculture, such as fruit monitoring or harvesting, requires perceiving the objects' spatial position. RGB-D cameras are limited under open-field environments due to lightning interferences. Therefore, in this study, we approach the use of Histogram Filters (Bayesian Discrete Filters) to estimate the position of tomatoes in the tomato plant. Two kernel filters were studied: the square kernel and the Gaussian kernel. The implemented algorithm was essayed in simulation, with and without Gaussian noise and random noise, and in a testbed at laboratory conditions. The algorithm reported a mean absolute error lower than 10 mm in simulation and 20 mm in the testbed at laboratory conditions with an assessing distance of about 0.5 m. So, the results are viable for real environments and should be improved at closer distances.

1. Introduction

Agriculture is a critical sector in the global economy. Farmers and the agro-food industry have been adapting to meet the demands of the worldwide population, which is increasing fast [10]. Several studies support that the population should keep increasing fast and reach about nine billion people by the year 2050 [7, 25]. Besides the increasing food demands to fulfil the global population [7], the area dedicated to agriculture can only increase marginally, requiring more optimised and precise strategies to improve production and cultivation ratios. These factors, associated with the labour shortage for agricultural tasks [13, 28], ally technology to farming and the agro-food industry.

Several scientific studies in the literature have been proving that robots can support farmers in agricultural tasks [6, 21, 31] and compensate for the labour shortage. Mobile and intelligent robots can successfully perform tasks such as monitoring and harvesting. However, these robots require dedicated sensors to perceive fruits and other objects and estimate their localisation to the tools.

Recent literature reviews proved that most works for perceiving fruits use RGB-D sensors [4, 11, 17, 24, 32]. However, most of these essays were performed under controlled lightening, ensuring the sensors' correct functioning [11]. RGB-D sensors tend to malfunction under open-field environments due to

reflections or intense illumination [8, 11, 29]. Therefore, using auxiliary algorithms and alternative technology is important to overcome the lightning effects.

Concerning estimating the depth using monocular cameras, most of the more recent works focused in Convolution Neural Networks to infer this relative depth to the sensor [14, 15, 23, 27, 34]. Mousavian *et al.* [23] used a Convolution Neural Network to estimate the three-dimension pose of an object and deployed a MultiBin loss function to optimise the model. Ma *et al.* [14, 15] deployed custom-made Convolution Neural Networks named MonoPointNet and PatchNet to generate three-dimension images from monocular images and detect objects. Also, Haq *et al.* [34] designed a new Regional Proposal Network with geometric constraints to detect three-dimension objects using monocular cameras. This architecture performed similarly to [14, 15]. Van and Do [35] used a chessboard background and a regression-based Convolution Neural Network to estimate the three-dimension pose of irregular objects using cuboids. The dependency on a chessboard background to predict the objects pose constraints on the applicability of the model for unstructured environments.

Other works used auxiliary sensors to create three-dimension scenes or depth estimation, such as Light Detection and Rangings [9]. However, high resolution and quality Light Detection and Rangings are expensive, and they increase the effort over robotic manipulators to manoeuvre and pick objects.

There are still some researchers that opted for using monocular cameras and controlling the path to the objects using visual servoing strategies [12, 26]. Shen *et al.* [32] applied visual servoing using RGB-D cameras. A distinctive work is presented by Xu *et al.* [36] which used the brightness of the environment and the movement of the camera to estimate the depth and reconstruct the structure of the colon during endoscopies.

Probabilistic algorithms are also capable of estimating the objects' poses accurately. Algorithms such as Bayesian Histogram Filters were explored in the literature to identify and localise objects in the scenes using different kinds of sensors. Bayesian Histogram Filters are commonly used in robotics for localisation navigation purposes [3, 22, 33], but their potentialities enable him for other aims such as identifying and localising other objects. Sarmiento *et al.* [30] applied region histogram filters to identify people, animals and other obstacles in the ultrawideband scene to avoid collisions and follow people. Also, Engin and Isler [5] used this algorithm to localise random objects. Márton *et al.* [19] used a histogram filter to complement the information provided by a state-of-the-art position estimator and accurately estimate the object's orientation.

1.1. System and requirements

Actual robotised greenhouses are usually operated by robots on trails [2]. However, these environments require the development of robot-specific environments and do not fit in the commonly operated greenhouses. Therefore, robots operating in the most common greenhouses should be composed of wheeled mobile robots. AgRob v16 from INESC TEC (Fig. 1) is a wheeled robot with the Clearpath Husky platform¹ and all-terrain wheels designed for operating under open-field and controlled agricultural environments. This robot is currently being essayed in Douro steep slope vineyards and tomato greenhouses. It has a perception and controlling head that gathers data and information from the environment for navigation and mapping. Additionally, the Robotis Manipulator-H was assembled at the backside to perform tasks in the cultivars, such as monitoring, pruning, or harvesting.

Perception for manipulation is usually performed by eye-in-hand techniques. The Robotis Manipulator-H can handle either monocular or RGB-D cameras. RGB-D cameras can percept the three-dimension pose of objects, but they are bigger and more difficult to handle. Besides, RGB-D cameras have difficulty perceiving and estimating the objects' depth in open-field environments due to natural lightning interferences [8, 11, 29]. Therefore, using monocular cameras, the manipulator can percept the

¹See Clearpath Robotics 2023. Husky – Unmanned Ground Vehicle. Online <https://clearpathrobotics.com/husky-unmanned-ground-vehicle-robot/> [Last accessed on May 12th, 2023]

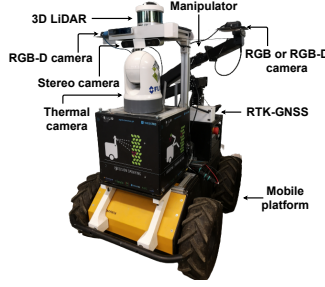


Figure 1: Robot AgRob v16 from INESC TEC to operate under open-field and controlled agricultural environments.

position of the objects from multiple perspectives and estimate the objects' pose. Approaches based on machine learning or statistics are commonly explored in the literature [14, 15, 23, 34], albeit statistical approaches are more analytical solutions and with more predictable results.

Therefore, as reviewed, Bayesian Histogram Filters are suitable for identifying the three-dimension position of objects and do not require the model's knowledge. So, for this work, we applied the histogram filter to identify the three-dimension position of tomatoes in a testbed using a monocular camera assembled in a robotic arm. The arm used fixed multi-viewpoint to observe the tomatoes from multiple perspectives.

The current work benefits, in our knowledge, for the first essay in using Bayesian Histogram Filters for estimating the three-dimension position of objects in the range of a robotic manipulator using monocular cameras. The implemented algorithm was evaluated under simulation and testbed conditions in the laboratory for fruit detection. Therefore, the current document innovates by:

- Firstly apply histogram filters to detect the centre position of objects;
- Apply the algorithm to real-world problems, such as the fruit detection in the plants' canopy; and
- Study the effect and advantages of different kernel types.

The following sections are structured: material and methods, results, discussion and conclusion. In section 2, we detail the conditions of the experiments and formalise the algorithm application. Section 3 introduces the different results for the different experiments, which are analysed, discussed and concluded in section 4.

2. Materials and Methods

2.1. Real data and simulation

The development and the experiments with the algorithm were done under two environments: simulation and a testbed in the laboratory (near real-world conditions).

A simplistic simulation environment was designed using the Ignition Gazebo Simulator². The scene comprises six spheres to assess the algorithm's validity and test during implementation (Fig. 2). The spheres have sizes of 5 cm and 10 cm. A bounding box camera was added to the scene to perceive the objects and support the position estimation algorithm. During the execution of the histogram filter, the bounding box camera is moved to fixed viewpoints to enable and validate the estimator. The bounding

²See Open Robotics, "Gazebo," accessed on May 12th, 2023. [Online]. Available: <https://gazebosim.org/>

box camera detects the objects through object detection algorithms using bounding boxes, detecting only their visible regions.

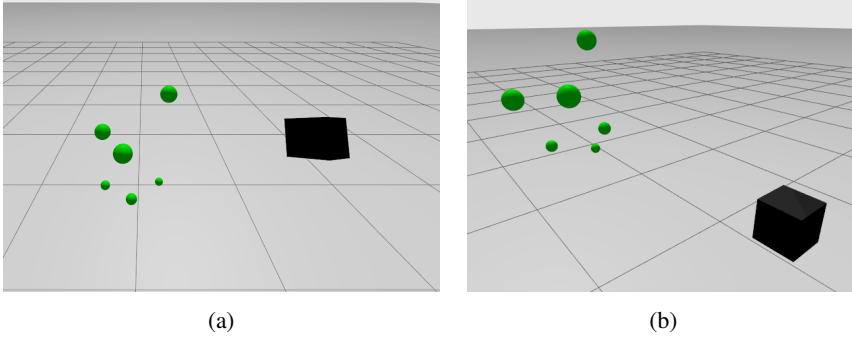


Figure 2: Simulated environment to validate the histogram filter effectiveness. Green spheres are the objects being detected, representing the tomatoes, and the black box is the bounding box camera looking at the spheres.

To essay the algorithm in the laboratory, near real-world greenhouse conditions, we designed a testbed with realistic leaves and plastic realistic tomatoes (Fig. 3a and 3b). For perceiving the tomatoes, we assembled an OAK-1 camera³ (Fig. 3d), as a bounding box camera, to the 6 degrees of freedom Robotis Manipulator-H (Fig. 3c). The OAK-1 camera computes an object detection model algorithm trained to perceive tomatoes. We used the You Only Look Once v8 tiny trained on the tomato dataset [16, 18] some sample of the plastic tomato from multiple perspectives. The manipulator also moved to fixed viewpoints that ensured the tomatoes' visibility. The manipulator was assembled on the mobile platform AgRob v16 from INESC TEC (Fig. 1), but three-dimension position of tomatoes was computed to the manipulator's base frame.

The OAK-1 is a fully integrated system for bounding box cameras. This camera was designed by the Luxonis Holding Corporation and has a single 12 MP RGB camera module. To allow the on-system object detection, the camera module is connected to the OAK-SoM⁴. The full camera connects to other devices through USB-C communication. The OAK-SoM is a system on module designed to integrate into top-level and low-power systems and has the capability to process artificial neural networks. This camera module was integrated into the AgRob v16 robot (Fig. 1).

This robot is based on the Clearpath Husky⁵ mobile platform and was designed to operate in harsh agricultural environments, such as the Douro's steep slope vineyards. At the front of the mobile platform, there is a controlling head, which is the unit with the computer and all the required devices to control the robot and establish communications. At the backside, the robot has the 6 degrees of freedom anthropomorphic manipulator Robotis Manipulator-H⁶.

³See Luxonis Holding Corporation, "OAK-1," accessed on September 26th, 2023. [Online]. Available: <https://docs.luxonis.com/projects/hardware/en/latest/pages/BW1093/>

⁴See Luxonis Holding Corporation, "OAK-SoM," accessed on September 26th, 2023. [Online]. Available: <https://docs.luxonis.com/projects/hardware/en/latest/pages/BW1099/>

⁵See Clearpath Robotics Inc., "Husky - Unmanned Ground Vehicle," accessed on September 26th, 2023. [Online]. Available: <https://clearpathrobotics.com/husky-unmanned-ground-vehicle-robot/>

⁶Robotis, "Robotis e-Manual – Manipulator-H," accessed on September 26th, 2023. [Online]. Available: https://emanual.robotis.com/docs/en/platform/manipulator_h/introduction/

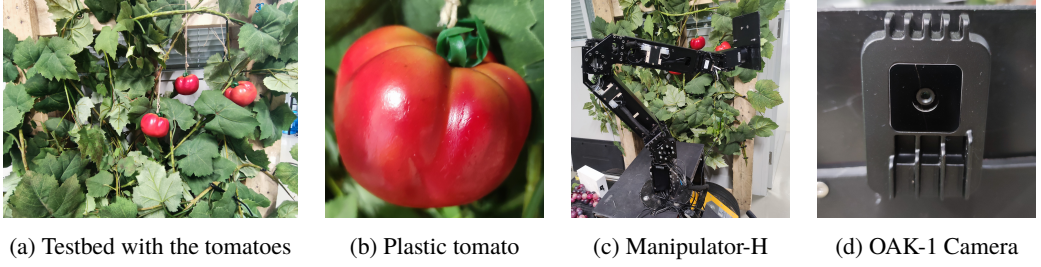


Figure 3: Simulated testbed in the laboratory to essay the histogram filter algorithm

2.2. Histogram Filter

Histogram filters have been widely used in literature for self-localisation and navigation in mobile robots [3, 22]. However, for the current study, we intend to apply histogram filters to localise the three-dimension position of tomatoes concerning the manipulator's base frame.

The histogram filter is a computationally intensive algorithm that can estimate the relative position of objects. The filter computes probabilities for multiple points in a discretised space. After, it intersects the chances of various views to estimate the localisation and the occupied area of the regions of interest (Fig. 4).

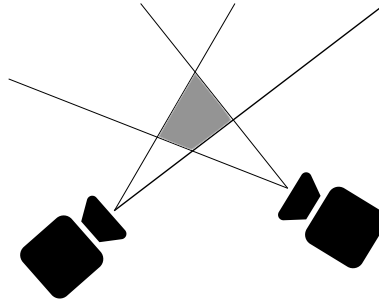


Figure 4: Intersection between multiple viewpoints in 2D plane

Histogram filters can be set as an application of a discrete Bayes filter to the continuous state space. For this study, we applied the histogram filter as stated by Thrun [33].

The histogram filter decomposes the continuous state space in a finite number of regions. Equation 1 describes a discretised state space. X_t is the random variable describing the state of the objects being detected at the time t . $\text{dom}(X_t)$ denotes the state space, which is all the possible values that X_t might assume. The most straightforward discretisation of a continuous state space is through a multidimensional grid, where $x_{k,t}$ denotes each cell of the grid.

$$\text{dom}(X_t) = x_{1,t} \cup x_{2,t} \cup \dots \cup x_{K,t} \quad (1)$$

Only part of the state space needs to be discredited to limit computation efforts, mainly due to the manipulator's reachability. Therefore, as soon as the manipulator's camera detects an object of interest, in the first viewpoint, the space behind the camera is decomposed through a grid scheme. We considered the probable space around the object as twice the manipulator's reaching limits. Twice the manipulator's reachability offers enough margin to identify and validate some fruits in the limits of the manipulator's reachability. The three-dimension decomposition is centred in the camera in yOz , i.e. in $(0, 0)$ in the

camera's frame and further distanced by the manipulator's reachability radius in Ox . Once decomposed, the discrete state space remains static and only $\text{dom}(X_t)$ is updated.

The histogram filter demands moving the camera to multiple strategic viewpoints and updating the probabilities grid. So, at the space decomposition, an associated probabilities matrix is created with a probability to each cell initialised to one, i.e. $\text{dom}(X_0) = [1 \dots 1]$. This means that at the beginning, the object of interest is probable to be anywhere in the decomposed space.

For estimating the position of the objects, $\text{dom}(X_t)$ is updated in each viewpoint. Each cell, $x_{i,t}$, from the decomposed state space is transformed from the manipulator's base frame to the image's frame. The probability of an object in a given cell, $x_{i,t}$, knowing the viewpoint, is given by (2). Finally, the updated probability of an object being in the cell $x_{i,t}$ is given by (3).

$$p(x_{i,t}|\text{viewpoint}_k) = \frac{1}{N} \sum_j^N p(x_{i,t}|\text{bbox}_j, \text{viewpoint}_k) \quad (2)$$

$$p(x_{i,t}) = p(x_{i,t}|\text{viewpoint}_k) \cdot p(x_{i,t-1}) \quad (3)$$

In equation 2, to get $p(x_{i,t}|\text{bbox}_j, \text{viewpoint}_k)$, a kernel function was designed. Two kernel functions were essayed to localise the objects in the state space: the square and Gaussian functions. The square kernel, applied to each bounding box, states that if the transformed point is inside a bounding box of the image's frame, the probability is one; otherwise is zero (4). Using the square kernel function, we will have a binary mask stating that if a point is inside the bounding box, then we can have an object. Otherwise, we don't.

$$p(x_{i,t}|\text{bbox}_j, \text{viewpoint}_k) = \begin{cases} 1 & \text{if inside bounding box} \\ 0 & \text{otherwise} \end{cases} \quad (4)$$

As an alternative to the aggressive behaviour of the square function, we also essayed the bidimensional Gaussian function (5). This function delivers a smooth effect for the borders of the bounding box and some cells $x_{i,t}$ outside the bounding boxes. Therefore, a Gaussian function should better tolerate irregular objects and noise. In the equation 5, (x_0, y_0) is the centre of bounding box j in the sensor's frame and (x, y) is the position of each cell $x_{i,t}$ in the sensor's frame. The coordinates in the image's frame are projected by a projection model stated in section 2.3. The standard deviation values (σ_x, σ_y) correspond to half of the size of the bounding box j . All the values were obtained experimentally and had reasonable results. If we use the Gaussian kernel (5) to estimate the objects' position, equation 2 will correspond to a mixture of Gaussians, attending that the detection camera detects multiple objects. The mixture of Gaussians results in a function that smooths with increasing Gaussians in the mixture. To avoid this effect, a normalised version of the mixture of Gaussians is used to highlight the different detected objects (6). Besides, the updated state space $\text{dim}(X_t)$ is also normalised at the end of each iteration of the histogram filter.

$$p(x_{i,t}|\text{bbox}_j, \text{viewpoint}_k) = \exp \left(-\frac{(x - x_0)^2}{2\sigma_x^2} - \frac{(y - y_0)^2}{2\sigma_y^2} \right) \quad (5)$$

$$p(x_{i,t}|\text{viewpoint}_k) = \frac{p(x_{i,t}|\text{viewpoint}_k)}{\max(p(x_{i,t}|\text{viewpoint}_k))} \quad (6)$$

The algorithm 1 summarises the procedures for updating the cell's weights during the histogram filtering.

Algorithm 1: Histogram filter – updating weights**Data:** *decomposition_grid*, *probabilities_matrix*, *bounding_boxes***Result:** *probabilities_matrix***for each viewpoint do** **for** $x_{i,t}, p(x_{i,t})$ **in** *decomposition_grid*, *probabilities_matrix* **do** $cell_camera \leftarrow$ transforms cell from the mainframe to camera's frame; $cell_sensor \leftarrow cell_camera$ in the sensor's frame; $(u, v) \leftarrow cell_sensor$ in the image's frame; $p(x_{i,t} | viewpoint_k) \leftarrow 0$; **for** $bbox$ **in** *bounding_boxes* **do** $p(x_{i,t} | viewpoint_k) \leftarrow p(x_{i,t} | viewpoint_k) + \frac{1}{N} \times p(x_{i,t} | bbox)$; **end** **end** $p(x_t | viewpoint_k) \leftarrow \text{normalise}(p(x_t | viewpoint_k))$; $p(x_t) \leftarrow p(x_t) \times p(x_t | viewpoint_k)$; $p(x_t) \leftarrow \text{normalise}(p(x_t))$;**end**

2.3. Camera Projection Model

While applying the histogram filter, we decomposed the state space in a finite state space grid. To effectively estimate the three-dimension position of the object, we moved the detection camera around the object and the decomposed state space to visualise the scene from multiple perspectives.

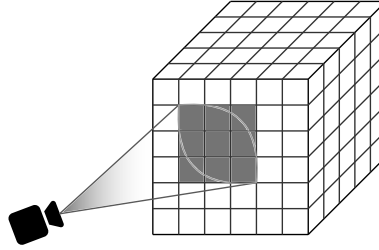


Figure 5: Intersection of the camera around in the decomposed space.

Detecting objects using the detection camera requires an effective projection model to estimate the object's position in the three-dimension space, transforming between the three-dimension space coordinates and the image's frame. For simplification, we applied the Pinhole model to transform the ac3D space coordinates to the image's frame.

Acknowledging the points of the 3D space in the camera's frame, before we project them in the image's frame, we have to convert them to the sensor's frame. Both are placed in the same origin, but they have different orientations. The sensor uses the frame as illustrated in Fig. 6. The illustrated rotation can be stated by Euler angles like Euler(YZX) = (0°, 90°, -90°) which reflects in the quaternion $q = (-0.5, 0.5, -0.5, 0.5)$.

The transformation between the sensor's frame and the image's coordinates can be made by the intrinsics parameters matrix as stated in equation 7. This matrix depends on the image's width (w)

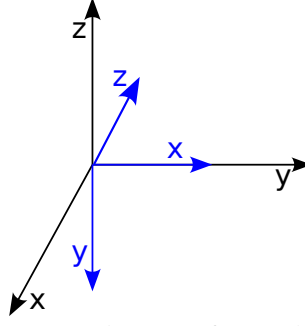


Figure 6: Conversion between the camera's and sensor's frames (blue – sensor's frame; black – camera's frame).

and height (h), as well as on the camera's focal length (f). The focal length depends on the camera's horizontal field of view and the image's width and can be calculated by equation 8.

$$(u, v, 1) = \begin{bmatrix} f & 0 & \frac{w}{2} \\ 0 & f & \frac{h}{2} \\ 0 & 0 & 1 \end{bmatrix} \cdot \begin{bmatrix} \frac{x}{z} \\ \frac{y}{z} \\ 1 \end{bmatrix} \quad (7)$$

$$f = \frac{0.5 \times w}{\tan\left(0.5 \times HFOV \times \frac{\pi}{180}\right)} \quad (8)$$

However, this model type is only valid behind ideal scenes, such as in the simulation. For the OAK-1 camera, an additional calibration step was required to estimate the intrinsic parameters. For calibration, we used the Kalibr software [20].

2.4. Objects positioning

At the end of the execution of the histogram filter for multiple viewpoints, the state space $\text{dom}(X_t)$ should have different clusters of points. As we know the number of objects in the scene through the number of detected objects by the detection camera, we can use the k-means algorithm to aggregate the points and compute the centre of each cluster.

The k-means algorithm tries to cluster the different points of the discrete state space by minimising the geometric distance between points to the cluster's centre (9). In the equation 9, we minimise the Euclidean distance between points to μ_j , the centre point of each cluster in C .

$$\sum_{i=0}^n \min_{\mu_j \in C} (||x_{i,t} - \mu_j||^2) \quad (9)$$

After clustering by the k-means, the state space should have as many point clouds as the number of objects detected by the detection camera. The computation of the centre of the clouds to get the position of the detected objects can be done in two ways:

1. computation of the geometric centre of the cloud; or
2. computation of the weighted centre of the cloud.

The geometric centre of each point cloud is the Euclidean centre μ_j minimised during the k-means algorithm for the equation 9. Besides the geometric centre, the k-means also return the points, $x_{i,t}$, that belong to each cloud, S_j . Considering the state of each element of the state space $\text{dom}(X_t)$ at the end of the histogram filter, each element $x_{i,t}$ should have a weight attributed, w_i . So the weighted centre is the weighted average (10) of the coordinates of $x_{i,t}$ that belong to the set S_j .

$$\mu_j = \left[\frac{\sum_i^N w_i \cdot x_{i,t_1}}{N} \quad \frac{\sum_i^N w_i \cdot x_{i,t_2}}{N} \quad \frac{\sum_i^N w_i \cdot x_{i,t_3}}{N} \right]^T \quad \forall x_{i,t} \in S_j \quad (10)$$

2.5. Experiments

Three essays were performed in different environments to validate the effectiveness of the histogram filter algorithm.

Using the Gazebo simulator, we created a scene with multiple spheres to estimate their position in the scene (Fig. 2). Once we used a bounding box camera without noise, this approach allowed validating the real performance of the filter without external artefacts or noise. Additionally, we performed an additional essay, introducing some Gaussian noise that randomly changes the position and size of the bounding box of the detected objects, as well as whether the object is successfully detected. Because we do not assemble any manipulator at the simulator, the bounding box camera has more freedom to state its pose. So, during the simulations, we set the camera's pose to ensure the spheres' visibility. Fig. 7 illustrates the visible image of the camera at each pose. In the first pose, the camera looks straight towards the spheres (Fig. 7a). After the camera moves down and left, looking upwards (Fig. 7b), and finally, the camera moves up and right to the first pose, looking downwards (Fig. 7c). This composition of the camera was kept for both experiments in the simulator.

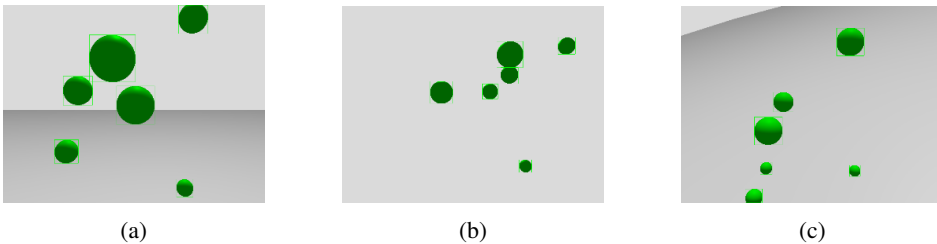


Figure 7: View of the spheres by the bounding box camera at each fixed viewpoint. The green square boxes around the spheres are the bounding boxes of the detected spheres by the bounding box camera.

In the third essay, a realistic testbed was deployed to experiment with the algorithm in near-real-world conditions at the laboratory (Fig. 3). The testbed is composed of realistic artificial leaves and realistic plastic tomatoes. The tomatoes were hung in the testbed between the leaves. For baselining the tomatoes' position in the testbed, we relied on the manipulator's kinematics. For each tomato in the testbed, we moved the manipulator end-effector until the fruit and retrieved the end-effector's position. This will be the tomato position to the manipulator's base frame. Similarly to the essays in simulation, the bounding box camera at the simulator moved to three fixed poses that always assured the visibility of the tomatoes. A similar scheme to the one used before was set concerning the several limitations of the manipulator's manoeuvrability that become difficult to set some poses to the camera. Fig. 8 illustrates the tomatoes' visibility by the OAK camera at each selected pose.

To better assess the performance of the histogram filter to estimate the position of objects, we extracted some error metrics, namely the mean absolute error (11), the mean square error (12), the

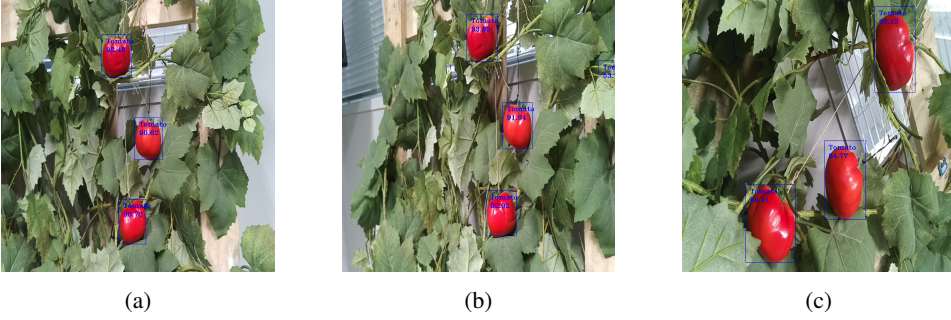


Figure 8: View of the tomatoes in the testbed at each pose of the OAK-1 camera. The blue squares around the tomatoes are the detected tomatoes by the bounding box camera OAK-1 using a custom-trained YOLO v8 tiny detector. Inside each bounding box are the detected class (tomato) and the detection confidence.

root mean square error or standard deviation (13). In these equations, μ_j is the real centre of the object for the cluster S_j , and $\hat{\mu}_j$ is the estimated one using the previous methods, given the cluster j until the maximum of clusters M .

$$MAE(\mu_j, \hat{\mu}_j) = \frac{1}{N \cdot M} \sum_i^N \sum_j^M |\mu_{ij} - \hat{\mu}_{ij}| \quad \forall j \in \mathbb{N} : \{1..M\} \quad (11)$$

$$MSE(\mu_j, \hat{\mu}_j) = \frac{1}{N \cdot M} \sum_i^N \sum_j^M (\mu_{ij} - \hat{\mu}_{ij})^2 \quad \forall j \in \mathbb{N} : \{1..M\} \quad (12)$$

$$RMSE(\mu_j, \hat{\mu}_j) = \sqrt{\frac{1}{N \cdot M} \sum_i^N \sum_j^M (\mu_{ij} - \hat{\mu}_{ij})^2} \quad \forall j \in \mathbb{N} : \{1..M\} \quad (13)$$

3. Results

As referred at the previous section, we made three essays to validate the algorithm performance. Two essays happened in simulation, while the third was in a simulated testbed at the laboratory. To measure the performance, we recurred to different error metrics: (11), (12) and (13). The manipulator and the bounding box camera were moved to fixed poses where all the fruits were always visible. All permutations between poses were considered for the essays, resulting in six estimations of each tomato for each experiment. The computed error results from the error of each estimated pose to each corresponding tomato.

In the first essay, we used the simulation to estimate the three-dimension position of the green spheres (Fig. 2) without any noise. During the execution of the histogram filter, the bounding box camera moved to different poses to intersect and be these positions. At each pose, the state space is operated to remove or smooth the existence of objects in each state according to the used kernel. Two kinds of kernels were considered, the square kernel (Fig. 9) and the Gaussian kernel (Fig. 10). Visually, both kernels performed similarly; however, the Gaussian kernel has two hyperparameters that deliver more freedom to set the kernel's size and estimate the objects' position, allowing the Gaussian filter to be more aggressive or smooth. We considered a two dimension Gaussian Filter with $\mathcal{N}(0, \text{size}/2)$ for the current experiment, where size is the width or the height of the detected object. The plot of Fig. 11 illustrates the error

considering using a square or Gaussian kernel and the geometric centres from the k-means algorithm or the weighted centre resulting from applying weights of the histogram filter. For this experiment, using a Gaussian kernel with a weighted centre estimation is advantageous.

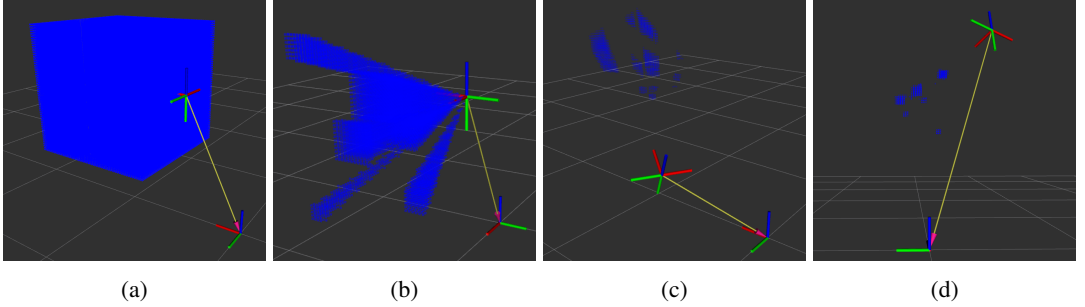


Figure 9: Iteration of the Histogram filter during simulation for detecting the six spheres, considering a square kernel. (a) decomposition of the state space at the beginning of the algorithm; (b) detection at the end of the first viewpoint; (c) detection at the end of the second viewpoint; (d) detection at the end of the third viewpoint.

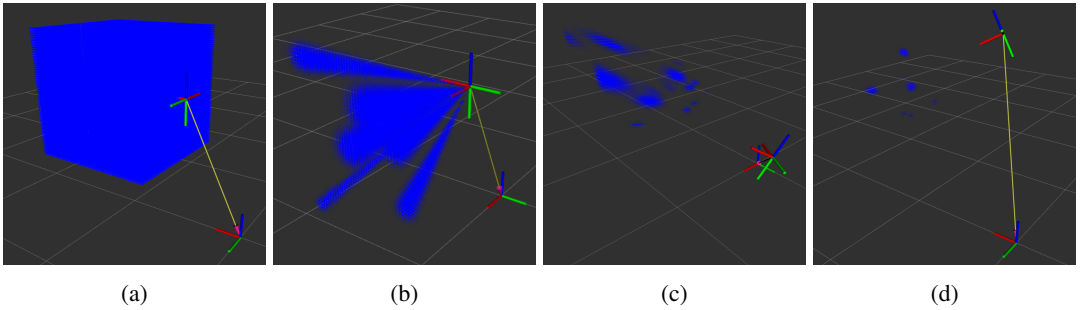


Figure 10: Iteration of the Histogram filter during simulation for detecting the six spheres, considering a gaussian kernel, $\mathcal{N}(0, 0.2)$. (a) decomposition of the state space at the beginning of the algorithm; (b) detection at the end of the first viewpoint; (c) detection at the end of the second viewpoint; (d) detection at the end of the third viewpoint.

Adding some noise to the simulation by moving the bounding box's centre and size and deleting it randomly, we get the results of Fig. 12. For moving the bounding box's centre and dimensions, we considered a Gaussian profile with $\mathcal{N}(0, 0.05)$. The bounding box will likely fail of 2 %. Once again, the Gaussian kernel with a weighted estimation of the spheres' centre performed better. Besides, in this experiment, the Gaussian kernel was more robust and accurate than the square kernel. The behaviour of the histogram filter in each pose is similar to the previous essay, but now, the algorithm has reported more noise. We set the Gaussian kernel such as $\mathcal{N}(0, size/3)$ to overcome this effect and have a more stable filter. This is the smallest value that assures that any fruit is lost and the point cloud is not too sparse, intersecting with the cloud of other fruits.

Given the overall success of the experiment with a mean absolute error smaller than 1 cm, we essayed the algorithm in a testbed at the laboratory. Fig. 13 illustrates the error of our system in the testbed using the Robotis Manipulator-H and the OAK-1 camera. In all the camera poses, all the tomatoes were always

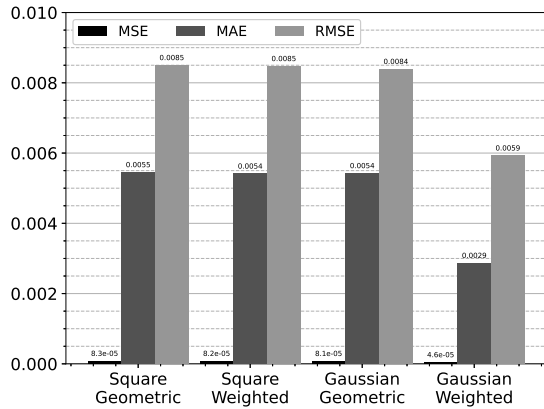


Figure 11: Error in estimating the position of the spheres in simulation without noise

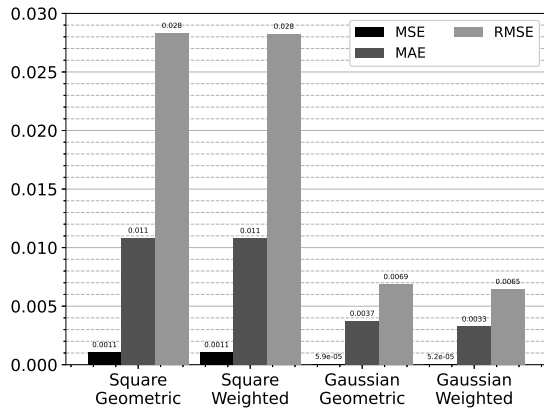


Figure 12: Error in estimating the position of the spheres in simulation with noise

visible (Fig. 8). Against the expected, Gaussian kernels performed worse than square kernels, and the results of weighted and geometric centres are identical.

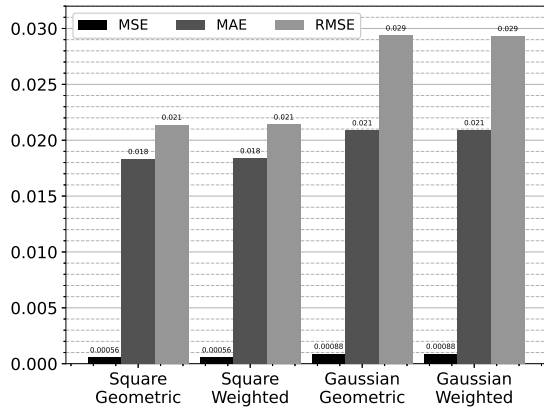


Figure 13: Error in estimating the position of the tomatoes at the testbed

4. Discussion

The overall use of histogram filters for estimating the three-dimension position of tomato fruits looks effective.

Under a simulated environment, the system always got a maximum error smaller than 10 mm. Increasing the resolution of the discretised state space could leverage better system accuracy, increasing the processing time and memory usage. As made in the second experiment, adding noise to the system makes the importance of using smooth kernels visible. The square kernel's aggressive binary behaviour rejects some state space positions and can never be recovered. On the other hand, the Gaussian filter has a smooth behaviour, and the positions are iteratively removed according to their distance from the filter's centre. So, smooth kernels can recover some state space points since they are never completely rejected. Besides, the Gaussian filter also was more failure-prone than the square kernel because the last one failed many times to detect the fruits, forcing to repeat the experiments. Because the positions near the centre of the tomato have a bigger score, using weighted centre estimation procedures allows for a better fit of the estimated centre to the real centre of the tomato, reducing the effect and deviations of sparse clouds.

When moving the implemented algorithm to a real robot and camera in a testbed, we reported that, against expectations, the Gaussian kernels were not very effective and square kernels reached a higher accuracy. In this case, it is always irrelevant to consider geometric or weighted estimations of the centre. In the testbed, the system reported a mean absolute error around 20 mm that can compromise the use of the algorithm for more demanding tasks. However, it is still important to better identify the source of the error, whether it comes from the algorithm or the baseline, that was badly fitted to the tomato centre. Although the experiment was made with the viewpoints distanced by around 0.5 m of the fruits, the error should improve if a closer assessment of the tomato position is made.

The histogram filter can estimate objects' position in the three-dimension, mainly the circular ones. However, this algorithm is computationally demanding and requires many resources and time to compute a solution. In our case, the system took about one minute in each pose to compute the decomposed state-space using an Intel Core i7 with 8 GB of Random-Access Memory. However, this is a highly parallelisable algorithm once all the positions are independent and can be computed simultaneously. So parallel implementation of the histogram filter at the Computer Processing Unit, Graphical Processing Unit, or mainly at the Field Programmable Gate Array can proportionally boost the speed of inference. Additionally, better optimisation of the implemented code can be done, mainly by using more efficient

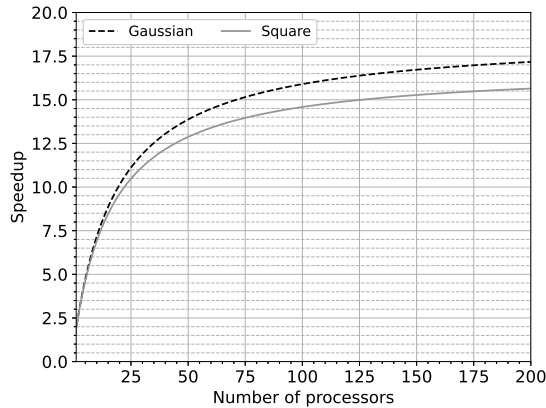


Figure 14: Maximum speedup analysis for parallelisation according to Amdahl's Law for the Gaussian and Square kernels.

programming languages such as C or C++ instead of Python, which is less efficient and is interpreted during execution.

To better understand the advantages of parallelising the histogram filter, we studied the algorithm speedup through Amdahl's law [1] (14). In this equation, (14), $\sigma(n)$ is the inherently sequential computations, $\varphi(n)$ is the potentially parallel computations, and p is the number of processors (processes computing in parallel). It is important to mind that Amdahl's law ignores the communications between processes, so this law only computes the maximum speedup, $\Psi(n, p)$. Fig. 14 illustrates the maximum reachable speedup by parallelising the histogram filter. The Gaussian filter reaches a higher speedup of about 17.5, but the square is a simpler kernel that operates faster, so the speedup is limited by the inherently sequential operations that cannot be optimised. During simulation, in a computer with an Intel Core i7 and 8 GB of Random-Access Memory, the histogram filter took about 115 s/pose using the Gaussian Filter and 99 s/pose using the square kernel, without parallelisation. The number of available cores also limits the speedup of the histogram filter. Once it is a very parallelisable algorithm, it benefits from using many cores, so the Computer Processing Unit is not so interesting such as Graphical Processing Unit or Field Programmable Gate Array, because it is usually limited to 16 cores.

$$\Psi(n, p) \leq \frac{\sigma(n) + \varphi(n)}{\sigma(n) + \frac{\varphi(n)}{p}} \quad (14)$$

5. Conclusion

During this experiment, we designed a histogram filter-based algorithm to infer the three-dimension position of tomatoes in the tomato plant canopy using monocular cameras. The algorithm performed reasonably with an overall error until 20 mm in laboratory-controlled conditions.

Despite the histogram filter being valid for estimating the tomatoes' position, some additional improvements are required. The further steps should focus on optimising the selection of the observation poses, making these poses adjustable and variable according to the fruit being analysed and maximising the observability. Besides, improvements in the execution time are still demanded by optimising the developed code and implementing parallelisation strategies.

Therefore, using histogram filters to estimate the position of objects is viable and suitable for operating in the field under controlled scenarios. Further essays for real scenarios should be performed, and the implementation of active perception strategies.

References

- [1] G. M. Amdahl. Validity of the single processor approach to achieving large scale computing capabilities. In *Proceedings of the April 18-20, 1967, spring joint computer conference on - AFIPS '67 (Spring) 1967*, pp. 483–485, Atlantic City New Jersey. ACM Press.
- [2] B. Arad, J. Balendonck, R. Barth, O. Ben-Shahar, Y. Edan, T. Hellström, J. Hemming, P. Kurtser, O. Ringdahl, T. Tielen, and B. van Tuijl. Development of a sweet pepper harvesting robot. *Journal of Field Robotics*, **37** (6), 1027–1039 (2020).
- [3] N. Boyko and Y. Hladun. Histogram Filter for Robot Localization. In *2021 IEEE 16th International Conference on Computer Sciences and Information Technologies (CSIT) 2021*, pp. 38–43, LVIV, Ukraine. IEEE.
- [4] G. Colucci, L. Tagliavini, A. Botta, L. Baglieri, and G. Quaglia. Decoupled motion planning of a mobile manipulator for precision agriculture. *Robotica*, **41** (6), 1872–1887 (2023).

- [5] S. Engin and V. Isler. Active Localization of Multiple Targets from Noisy Relative Measurements. In *Algorithmic Foundations of Robotics XIV 2021*, volume 17 of *Springer Proceedings in Advanced Robotics*, pp. 398–413. Springer International Publishing.
- [6] euRobotics 2014. Strategic Agenda for Robotics in Europe. resreport.
- [7] Food and Agriculture Organization of the United States 2023. FAOSTAT Statistical Database. Accessed on March 21st, 2023.
- [8] J. Gené-Mola, J. Llorens, J. R. Rosell-Polo, E. Gregorio, J. Arnó, F. Solanelles, J. A. Martínez-Casasnovas, and A. Escolà. Assessing the Performance of RGB-D Sensors for 3D Fruit Crop Canopy Characterization under Different Operating and Lighting Conditions. *Sensors*, **20** (24), 7072 (2020).
- [9] G. Iyer, R. K. Ram, J. K. Murthy, and K. M. Krishna. CalibNet: Geometrically Supervised Extrinsic Calibration using 3D Spatial Transformer Networks. In *2018 IEEE/RSJ International Conference on Intelligent Robots and Systems (IROS) 2018*, Madrid, Spain. IEEE.
- [10] J. Kitzes, M. Wackernagel, J. Loh, A. Peller, S. Goldfinger, D. Cheng, and K. Tea. Shrink and share: humanity’s present and future Ecological Footprint. *Philosophical Transactions of the Royal Society B: Biological Sciences*, **363** (1491), 467–475 (2007).
- [11] M. S. Kumar and S. Mohan. Selective fruit harvesting: Research, trends and developments towards fruit detection and localization — A review. *Proceedings of the Institution of Mechanical Engineers, Part C: Journal of Mechanical Engineering Science*, **237** (6), 1405–1444 (2022).
- [12] H. Küçük, G. Parker, and E. T. Baumgartner. Robot positioning of flexible-link manipulator using vision. *Robotica*, **22** (3), 301–307 (2004).
- [13] M. Leshcheva and A. Ivolga. Human resources for agricultural organizations of agro-industrial region, areas for improvement. In *Sustainable agriculture and rural development in terms of the Republic of Serbia strategic goals realization within the Danube region: support programs for the improvement of agricultural and rural development 2017*, pp. 386–400, Belgrade, Serbia. Institute of Agricultural Economics.
- [14] X. Ma, S. Liu, Z. Xia, H. Zhang, X. Zeng, and W. Ouyang. Rethinking Pseudo-LiDAR Representation. In *Computer Vision – ECCV 2020 2020*, volume 12358 of *Lecture Notes in Computer Science*, pp. 311–327, Online. Springer International Publishing.
- [15] X. Ma, Z. Wang, H. Li, P. Zhang, W. Ouyang, and X. Fan. Accurate Monocular 3D Object Detection via Color-Embedded 3D Reconstruction for Autonomous Driving. In *2019 IEEE/CVF International Conference on Computer Vision (ICCV) 2019*, pp. 6850–6859, Seoul, Korea (South). IEEE.
- [16] S. A. Magalhães, L. Castro, G. Moreira, F. N. dos Santos, M. Cunha, J. Dias, and A. P. Moreira. Evaluating the Single-Shot MultiBox Detector and YOLO Deep Learning Models for the Detection of Tomatoes in a Greenhouse. *Sensors*, **21** (10), 3569 (2021).
- [17] S. A. Magalhães, A. P. Moreira, F. N. dos Santos, and J. Dias. Active Perception Fruit Harvesting Robots — A Systematic Review. *Journal of Intelligent & Robotic Systems*, **105** (14) (2022).
- [18] S. A. Magalhães 2020. Dataset of tomato inside greenhouses for object detection in Pascal VOC. Online. Last accessed on April 27th, 2023.
- [19] Z. C. Márton, S. Türker, C. Rink, M. Brucker, S. Kriegel, T. Bodenmüller, and S. Riedel. Improving object orientation estimates by considering multiple viewpoints. *Autonomous Robots*, **42** (2), 423–442 (2017).
- [20] J. Maye, P. Furgale, and R. Siegwart. Self-supervised calibration for robotic systems. In *2013 IEEE Intelligent Vehicles Symposium (IV) 2013*, pp. 473–480, Gold Coast, QLD, Australia. IEEE.
- [21] A. McBratney, B. Whelan, T. Ancev, and J. Bouma. Future Directions of Precision Agriculture. *Precision Agriculture*, **6**, 7–23 (2005).
- [22] A. Moscowsky. Subdefinite Computations for Reducing the Search Space in Mobile Robot Localization Task. In *Artificial Intelligence 2021*, volume 12948 of *Lecture Notes in Computer Science*, pp. 180–196. Springer International Publishing.

- [23] A. Mousavian, D. Anguelov, J. Flynn, and J. Kosecka. 3D Bounding Box Estimation Using Deep Learning and Geometry. In *2017 IEEE Conference on Computer Vision and Pattern Recognition (CVPR)* 2017. IEEE.
- [24] S. R. Nekoo, D. Feliu-Talegon, R. Tapia, A. C. Satue, J. R. M. de Dios, and A. Ollero. A 94.1 g scissors-type dual-arm cooperative manipulator for plant sampling by an ornithopter using a vision detection system. *Robotica*, **41** (10), 3022–3039 (2023).
- [25] M. Perry. Science and Innovation Strategic Policy Plans for the 2020s (EU,AU,UK): Will They Prepare Us for the World in 2050? *Applied Economics and Finance*, **2** (3) (2015).
- [26] J. Qu, F. Zhang, Y. Fu, and S. Guo. Multi-cameras visual servoing for dual-arm coordinated manipulation. *Robotica*, **35** (11), 2218–2237 (2017).
- [27] R. Ranftl, K. Lasinger, D. Hafner, K. Schindler, and V. Koltun. Towards robust monocular depth estimation: Mixing datasets for zero-shot cross-dataset transfer. *IEEE Transactions on Pattern Analysis and Machine Intelligence*, **44** (3), 1623–1637 (2022).
- [28] R. L. V. Rica, G. G. Delan, E. V. Tan, and I. A. Monte. Status of Agriculture, Forestry, Fisheries and Natural Resources Human Resource in Cebu and Bohol, Central Philippines. *Tropical Technology Journal*, **19** (11) (2015).
- [29] O. Ringdahl, P. Kurtser, and Y. Edan. Performance of RGB-D camera for different object types in greenhouse conditions. In *2019 European Conference on Mobile Robots (ECMR)* 2019, pp. 1–6, Prague, Czech Republic. IEEE.
- [30] J. Sarmiento, F. N. D. Santos, A. S. Aguiar, H. Sobreira, C. V. Regueiro, and A. Valente. FollowMe - A Pedestrian Following Algorithm for Agricultural Logistic Robots. In *2022 IEEE International Conference on Autonomous Robot Systems and Competitions (ICARSC)* 2022, pp. 179–185, Santa Maria da Feira, Portugal. IEEE.
- [31] A. Schmitz and C. B. Moss. Mechanized agriculture : machine adoption, farm size, and labor displacement. *AgBioForum*, **18** (3), 278–296 (2015).
- [32] J. Shen and N. Gans. Robot-to-human feedback and automatic object grasping using an RGB-D camera–projector system. *Robotica*, **36** (2), 241–260 (2017).
- [33] S. Thrun, W. Burgard, and D. Fox 2005. *Probabilistic robotics*. Intelligent Robotics and Autonomous Agents series. MIT Press.
- [34] Q. M. ul Haq, M. A. Haq, S.-J. Ruan, P.-J. Liang, and D.-Q. Gao. 3D Object Detection Based on Proposal Generation Network Utilizing Monocular Images. *IEEE Consumer Electronics Magazine*, **11** (5), 47–53 (2022).
- [35] X. H. Van and N. Do. An efficient regression method for 3D object localization in machine vision systems. *IAES International Journal of Robotics and Automation (IJRA)*, **11** (2), 111–121 (2022).
- [36] L. Xu, J. Li, Y. Hao, P. Zhang, G. Ciuti, P. Dario, and Q. Huang. Depth Estimation for Local Colon Structure in Monocular Capsule Endoscopy Based on Brightness and Camera Motion. *Robotica*, **39** (2), 334–345 (2020).

Author Contributions. Conceptualization, S.C.M. and F.N.d.S.; funding acquisition, S.A.M and F.N.d.S.; investigation, S.C.M.; methodology, S.C.M.; software, S.C.M.; formal analysis, S.C.M.; resources, F.N.d.S and A.P.M.; project administration, S.A.M, F.N.d.S., J.D. and A.P.M; supervision, F.N.d.S., J.D. and A.P.M.; validation, F.N.d.S., J.D. and A.P.M.; writing—original draft, S.C.M.; writing—review and editing, S.C.M., F.N.d.S., J.D. and A.P.M.

Financial Support. Sandro Costa Magalhães is granted by the Portuguese Foundation for Science and Technology (FCT) under scholarship agreement SFRH/BD/147117/2019.

Conflicts of Interest. The authors declare no conflicts of interest exist.

Ethical Approval. Not applicable.